Vol 17 No 3, March 2008
1674-1056/2008/17(03)/0978-10

Chinese Physics B

© 2008 Chin. Phys. Soc.
and IOP Publishing Ltd

Fifth-order phase-sensitive detection of ultrafast polarization beats in cascade four-level system*

Nie Zhi-Qiang(聂志强)[a], Li Pei-Zhe(李沛哲)[a], Yu Xiao-Jun(余孝军)[a], Zhang Yan-Peng(张彦鹏)[a)b)†], Jiang Tong(姜 彤)[a], Li Ling(李 岭)[a], Gan Chen-Li(甘琛利)[b], Zuo Cui-Cui(左翠翠)[a], Zhang Peng-Fei(张鹏飞)[a], Song Jian-Ping(宋建平)[a], and Lu Ke-Qing(卢克清)[c]

[a] *Key Laboratory for Physical Electronics and Devices of the Ministry of Education, Xi'an Jiaotong University, Xi'an* 710049, *China*

[b] *Department of Physics, University of Arkansas, Fayetteville, Arkansas* 72701, *USA*

[c] *State Key Laboratory of Transient Optics and Technology, Xi'an Institute of Optics and Precision Mechanics, Chinese Academy of Sciences, Xi'an* 710068, *China*

(Received 9 June 2007; revised manuscript received 10 October 2007)

We study the colour-locked twin-noisy-field correlation effects in the fifth-order nonlinear susceptibility of ultrafast polarization beats in a cascade four-level system. More importantly, the fifth-order phase-sensitive heterodyne detection of ultrafast polarization beats has been exploited. The fifth-order nonlinear optical response can be controlled and modified through the colour-locked correlation of twin noisy fields. Thus, this method with the phase dispersion information is a good way to measure the real and imaginary parts of the fifth-order nonlinear susceptibility.

Keywords: ultrafast polarization beat, nonlinear susceptibility, phase-sensitive detection
PACC: 4265, 3280

1. Introduction

In the past few years, atomic coherence effects in multi-level atomic systems have attracted great attention and many studies on nonlinear optical interference effect have been carried out both theoretically and experimentally.[1−9] Ultrafast polarization beats are an important nonlinear effect involving interference between macroscopic polarizations which are excited simultaneously in the medium. With laser pulse of ns timescale duration, femto- or atto-second timescale modulations were observed.[10,11] As a time-domain technique, the main advantage of the ultrafast polarization technique over the conventional quantum beat technique is that the temporal resolution is not limited by the laser pulse width. Thus, we can control and modify nonlinear optical properties of an atomic medium through the colour-locked correlation of twin noisy driving fields.

Owing to the atomic coherence effect, the absorption and dispersion properties of the fifth-order polarization beats can be controlled by the time delay (τ) between two pump beams, and this is known as heterodyne detection. Coherent heterodyne detection is now widely used to detect weak scattered or reflected radiation in many electromagnetic spectral regions including radio wave, microwave, infrared, and optical spectra. In the optical region, heterodyne detection has been used in coherent laser radar, communications, spectroscopy, and radiometry due to its advantages, i.e. high sensitivity, frequency selectivity, and strong directionality. As a detection technique, the heterodyne detection can measure the amplitude and the phase of an incident signal field.

In this paper, we study the fifth-order complex susceptibility of the three-photon six-wave mixing (SWM) in femtosecond polarization beat (FSPB) in a cascade four-level system. FSPBs are induced by two-photon nondegenerate four-wave mixing (NDFWM) and SWM. We present a novel type of phase-sensitive

*Project supported by the National Natural Science Foundation of China (Grant Nos 60308002 and 60678005), the Foundation for the Author of National Excellent Doctoral Dissertation of China (Grant No 200339), the Foundation for Key Program of Ministry of Education, China (Grant No 105156), the Fok Ying-Tong Education Foundation for Young Teachers in the Higher Education Institutions of China (Grant No 101061) and the Specialized Research Fund for the Doctoral Program of Higher Education of China (Grant No 20050698017).

†Corresponding author. E-mail: ypzhang@mail.xjtu.edu.cn

detection, which is somewhat the same as the heterodyne detection. Through changing the time delay τ between two pump beams of NDFWM and SWM, we can adjust their relative phase. When the τ-dependent phase difference approaches to $2n\pi$ or $(2n+1/2)\pi$, the femtosecond polarization beat signal evolves into the nonlinear dispersion or absorption of fifth-order susceptibility. The reference signal is the NDFWM signal and it propagates in a little different direction. The SWM and the reference NDFWM signals then interfere directly between them at the detector. Our heterodyne detection is based on the femtosecond polarization interference between the SWM and NDFWM processes and this method is a good way to measure the fifth-order susceptibility directly.

2. Basic theory

2.1. Liouville pathways

A cascade four-level atomic system consists of one ground state $|0\rangle$, two intermediate states $|1\rangle$, $|2\rangle$ and one excited state $|3\rangle$. States between $|0\rangle$ and $|1\rangle$, $|1\rangle$ and $|2\rangle$, $|2\rangle$ and $|3\rangle$ are coupled through dipole transitions with resonant frequencies Ω_1, Ω_2 and Ω_3 respectively, while other transitions are dipole forbidden (Fig.1(a)). In Fig.1(b), beams 2 consists of two frequency components ω_2 and ω_3, beam 3 has only one frequency ω_2 and beam 1 also has only one frequency ω_1. We further assume that $\omega_1 \approx \Omega_1$, $\omega_2 \approx \Omega_2$ and $\omega_3 \approx \Omega_3$, therefore ω_1, ω_2 and ω_3 will drive the transitions from $|0\rangle$ to $|1\rangle$, $|1\rangle$ to $|2\rangle$ and $|2\rangle$ to $|3\rangle$, respectively (Fig.1(a)). There are two distinct processes involved in this system. First, the ω_1 frequency component of beam 1 and the ω_2 frequency component of beam 2 induce a two-photon coherence between levels $|0\rangle$ and $|2\rangle$ (only the ket is promoted to creating a coherence rather than a population), which is then probed by the ω_2 frequency component of the beam 3. This is a two-photon NDFWM ($|0\rangle \xrightarrow{\omega_1} |1\rangle \xrightarrow{\omega_2} |2\rangle \xrightarrow{-\omega_2} |1\rangle$) with a resonant intermediate state and the frequency of the signal being ω_1. The two-photon NDFWM process indicates that the ket is promoted to the excited state $|2\rangle$ by two field actions, one probe photon ω_2 is emitted, and then one phase-matching coherent photon ω_1 is emitted along the beam 4 direction (Fig.1(b)). Second, on the basis of two-photon NDFWM process, the ω_3 frequency component of beam 2 induces a three-photon coherence between levels $|0\rangle$ and $|3\rangle$, which is then probed by the ω_3 frequency component of the beam 2 and the ω_2 frequency component of beam 3. This is a three-photon SWM ($|0\rangle \xrightarrow{\omega_1} |1\rangle \xrightarrow{\omega_2} |2\rangle \xrightarrow{\omega_3} |3\rangle \xrightarrow{-\omega_3} |2\rangle \xrightarrow{-\omega_2} |1\rangle$) and the frequency of the signal equals ω_1 again. The three-photon SWM process indicates that the ket is promoted to the excited state $|3\rangle$ by three field actions, two probe photons ω_3 and ω_2 are emitted, and then one phase-matching coherent photon ω_1 is finally emitted along the beam 4 direction (Fig.1(b)). In this cascade four-level atomic system (Fig.1(a)), both polarizations have the same frequencies and the polarization interference of two excitation paths $|0\rangle \rightarrow |1\rangle \rightarrow |2\rangle \rightarrow |1\rangle$ (two-photon NDFWM) and $|0\rangle \rightarrow |1\rangle \rightarrow |2\rangle \rightarrow |3\rangle \rightarrow |2\rangle \rightarrow |1\rangle$ (three-photon SWM) leads to a femtosecond polarization beat (FSPB) phenomenon[10−12] in the homogeneously broadened sample.

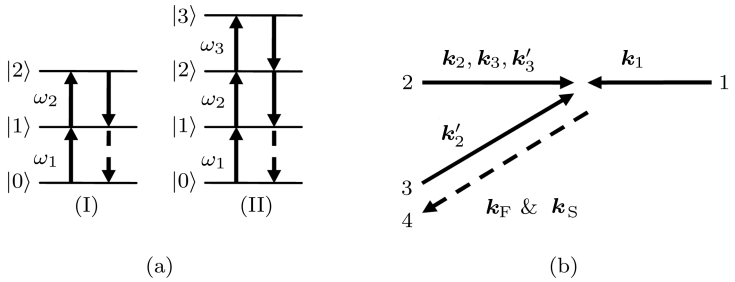


Fig.1. The ladder diagrams of three-state two-photon NDFWM and four-state three-photon SWM for perturbation chains I and II in Liouville space (a) and Phase-conjugation geometry of FSPB (b), where the solid and dash vertical lines correspond to ket interaction and signals of NDFWM and SWM respectively, with time evolving from left to right.

The twin composite stochastic fields of beam 2 ($E_{\rm p2}$) and beam 3 ($E_{\rm p3}$) can be written as

$$\begin{aligned} E_{\rm p2} &= E_2 + E_3 + E_3' \\ &= \varepsilon_2 u_2(t)\exp[{\rm i}(\boldsymbol{k}_2\cdot\boldsymbol{r}-\omega_2 t)] \\ &\quad +\varepsilon_3 u_3(t)\exp[{\rm i}(\boldsymbol{k}_3\cdot\boldsymbol{r}-\omega_3 t)] \\ &\quad +\varepsilon_3' u_3'(t-\tau)\exp[{\rm i}(\boldsymbol{k}_3'\cdot\boldsymbol{r}-\omega_3 t+\omega_3\tau)], \quad (1) \\ E_{\rm p3} &= E_2' \\ &= \varepsilon_2' u_2'(t-\tau)\exp[{\rm i}(\boldsymbol{k}_2'\cdot\boldsymbol{r}-\omega_2 t+\omega_2\tau)], \quad (2) \end{aligned}$$

where ε_i and $k_i(\varepsilon_i',\ k_i')$ $(i=2,3)$ are the constant field amplitudes and the wave vectors of the ω_i component without (with) time delay in beams; $u_i(t)$ is a dimensionless statistical factor that contains fluctuations in phase and in amplitude, and it is taken to be a complex ergodic stochastic function of t, which obeys complex circular Gaussian statistics in chaotic field; τ is the relative time delay between the prompt (unprimed) and the delayed (prime) fields. To accomplish this arrangement the frequency components of ω_2 and ω_3 lights are split and then recombined to provide beams 2 and 3. On the other hand, beam 1 is assumed to be quasi-monochromatic light ($u_1(t)\approx 1$), the complex electric field of beam 1 can be written as $E_{\rm p1}=\varepsilon_1 u_1(t)\exp[{\rm i}(\boldsymbol{k}_1\cdot\boldsymbol{r}-\omega_1 t)]$, where, ω_1, ε_1 and $\boldsymbol{k}_1$ are the frequency, the field amplitude and the wave vector, respectively. The FSPB scheme diagram is shown in Fig.1(b).

The atomic polarization and population equations of motion (atomic response) are considered to have the terms with different orders of Liouville pathways. To simplify the mathematics, we neglect the ground-state depletion ($\rho_{00}^{(0)}\approx 1$) and do not consider the propagation characteristics of the pulsed pump, probe and signal fields. Also, we retain only the resonant dipole interaction terms in the derivation of the complex susceptibility, which is known as the rotating-wave approximation (RWA). Because of the selectivity imposed by the RWA, each pulse interaction contributes in a unique way to the phase-matching direction of the nonlinear signal. We shall employ the perturbation theory to calculate the density-matrix elements in the following perturbation chains (Fig.2):

$$\begin{aligned} &\text{(I)}\ \rho_{00}^{(0)} \xrightarrow{E_1} \rho_{10}^{(1)} \xrightarrow{E_2} \rho_{20}^{(1)} \xrightarrow{(E_2')^*} \rho_{10}^{(2)}, \\ &\text{(II)}\ \rho_{00}^{(0)} \xrightarrow{E_1} \rho_{10}^{(1)} \xrightarrow{E_2} \rho_{20}^{(1)} \xrightarrow{E_3} \rho_{30}^{(2)} \xrightarrow{(E_3')^*} \rho_{20}^{(1)} \\ &\qquad \xrightarrow{(E_2')^*} \rho_{10}^{(2)}. \end{aligned}$$

Chain I corresponds to the two-photon NDFWM process, while chain II corresponds to the three-photon SWM process. They have phase-matching conditions $\boldsymbol{k}_{\rm S1}=\boldsymbol{k}_1+\boldsymbol{k}_2-\boldsymbol{k}_2'$ and $\boldsymbol{k}_{\rm S2}=\boldsymbol{k}_1+\boldsymbol{k}_2+\boldsymbol{k}_3-\boldsymbol{k}_3'-\boldsymbol{k}_2'$, respectively. As there exists a little angle between the directions of NDFWM and SWM, the interference between them leads to the spatial oscillation. Physically, NDFWM is the sum of two grating diffraction contributions, i.e. one is the large-angle moving grating induced by ω_1 and ω_2, and the other is the small-angle static grating induced by ω_2 and $-\omega_2$, while SWM comes from the sum of the four grating diffraction contributions i.e. one small-angle static grating induced by ω_3 and $-\omega_3$, two small-angle moving gratings induced by ω_2 and ω_3 and by $-\omega_2$ and $-\omega_3$, and one large-angle moving grating induced by ω_1 and ω_2.

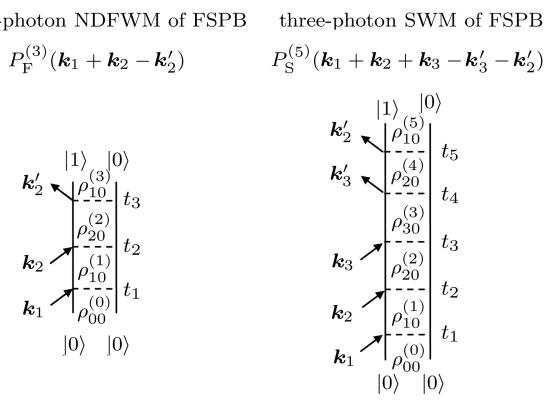


Fig.2. Two-photon NDFWM and three-photon SWM of FSPB. The left and the right vertical lines represent the ket and the bra, respectively; the applied electric fields are indicated with arrows oriented towards the right or the left if propagating with a positive wave vector or a negative wave vector respectively. Time evolves from the bottom to the top of the diagram.

The third-order and the fifth-order response functions ($\rho_{10}^{(3)}$ and $\rho_{10}^{(5)}$) of the perturbation chains I and II are given by using double-sided Feynman diagrams (DSFDs) in Fig.2 respectively. The time evolutions of the density-matrix elements of the optically driven atoms or molecules can be represented schematically by either the Liouville space coupling representation (chains I and II), the DSFDs (Fig.2), or the ladder diagrams (Fig.1(a)). In the Liouville space coupling representation (chains I and II), the state of the system is designated by a position in Liouville space, with indices corresponding to the ket-bra 'axis'. Up and down transitions on the ket are excited by positive and negative frequency fields respectively, whereas negative and positive frequency fields induce up and down transitions on the bra respectively. The DSFDs shown

in Fig.2 can be described as follows: the left and the right vertical lines of the diagram represent the time evolutions of the ket and bra, respectively; the applied electric fields are indicated with arrows oriented toward the left if propagating with a negative wave vector and toward the right for a positive wave vector. Each interaction with the electric field produces a transition between the two electronic states of either the bra or the ket. The ladder diagrams are shown in Fig.1(a). In this representation, the solid lines correspond to the ket interaction. The ability to trace the evolutions of the bra and the ket simultaneously makes the density matrix representation a most appropriate tool for describing many dynamical phenomena in nonlinear optical processes.

2.2. Colour-locking stochastic correlation

As is well known, lasers are inherently noisy devices and the phase and amplitude of the field can fluctuate in them. Therefore a noisy laser offers us a unique alternative to the conventional frequency-domain cw spectroscopy and ultrashort pulse time-domain spectroscopy, and it can be used to probe atomic and molecular dynamics. Colour-locked noisy light technique is an intermediate way between cw and short-pulse methods, and this technique results in the complete cancellation of the spectrally broad noise carried by the noisy light beams.[13] The fundamental difference between them is that the transform-limited femtosecond laser pulse is phase coherent (phase locked) while noisy light is phase random and non-transform limited. For the 'biatomic' model[13] of a macroscopic system where phase matching takes place, the NDFWM and SWM signals must be drawn from the third-order polarization $P_{\rm F}^{(3)}$ and the fifth-order polarization $P_{\rm S}^{(5)}$ (having time variable t) developed on one 'atom' multiplied by $(P_{\rm F}^{(3)})^*$ and $(P_{\rm S}^{(5)})^*$ (having time variable s) that are developed on another 'atom' which must be located elsewhere in space (with summation over all such pairs). Generally, we assume that the homodyne-detected FSPB signal intensity is proportional to the average of the absolute square of the sum of the third-order and the fifth-order polarization ($P = P_{\rm F}^{(3)} + P_{\rm S}^{(5)}$) over the random variable of the stochastic process $< |P|^2 >$ (having both t and s time variables), which involves the fourth- and the eighth-order coherence functions of $u_i(t)$ in phase-conjugation geometry. Unlike the second-order and the fourth-order coherence functions at the field-level averaging, the expansions of the fourth- and the eighth-order coherence functions at the intensity-level averaging strongly depend on three different Markovian noisy fields, i.e. chaotic field, phase-diffusion field, and Gaussian-amplitude field. When the FSPB signal is dominated in the case in which $u_2(t)$ and $u_3(t)$ (field 1 is quasi-monochromatic) field actions on single atom are correlated and the cross-atom-correlated actions are not important (which is usually true for atomic vapour systems), the FSPB signal intensity can be approximated by the absolute square of the non-trivial stochastic average of the polarization $|< P >|^2$ (averaging at the field level), which involves only the second- and the fourth-order coherence functions of $u_i(t)$. This works because for this particular spectroscopic technique the τ-dependent terms have only intra-atomic correlations but no inter-atomic correlations in the τ-dependent terms. In dealing with the gas-phase atomic medium, we make an approximation by averaging at the field level, which only needs the second- and the fourth-order correlation functions for the noise fields. The spatiotemporal second-order coherence function of noisy field is $< u_i(t_1)u_i^*(t_2) >= \exp(-\alpha_i\,|t_1 - t_2|)$ for a Lorentzian line shape. Here, $\alpha_i = \dfrac{1}{2}\delta\omega_i$ with $\delta\omega_i$ being the line width of ω_i frequency component, is the autocorrelation decay of the noisy field. On the other hand, noisy light is colour-locked; because each colour is coherent only with itself (it is uncorrelated with any other colour).

For a Doppler-broadened atomic system, the nonlinear polarizations $P_{\rm F}$ and $P_{\rm S}$ responsible for the phase-conjugate FWM and SWM signals are given by stochastic averaging over the velocity distribution function $w(\boldsymbol{v}) = \exp[-(v/u)^2]/\sqrt{\pi}u$, where $\boldsymbol{v}$ is the atomic velocity, $u = \sqrt{2\boldsymbol{k}_{\rm B}T/m}$ with m being the mass of an atom, $k_{\rm B}$ is Boltzmann constant and T the absolute temperature. The polarizations of NDFWM and SWM are given in the bare-state basis. $P_{\rm F}(\boldsymbol{v},t)$ and $P_{\rm S}(\boldsymbol{v},t)$ correspond to the third-order and the fifth-order polarizations of the perturbation chains I and II, respectively. The formulas below indicate how the initial density-matrix elements are transformed into higher-order elements through interactions with the electric fields:

$$\begin{aligned} P_{\rm F}(\boldsymbol{v},t) &= N\mu_1 \int {\rm d}\boldsymbol{v} w(\boldsymbol{v}) \rho_{10}^{(3)}(\boldsymbol{v}) \\ &= A \int w(\boldsymbol{v}) \exp\left[-{\rm i}\theta^{({\rm I})}\right] H_1(t_1) H_2(t_2) H_3(t_3) \\ &\quad \times < u_2(t - t_2 - t_3) u_2^*(t - t_3 - \tau) > {\rm d}\Sigma_1, \end{aligned} \tag{3}$$

$$
\begin{aligned}
P_{\rm S}(\boldsymbol{v},t) &= N\mu_1 \int {\rm d}\boldsymbol{v} w(\boldsymbol{v}) \rho_{10}^{(5)}(\boldsymbol{v}) \\
&= B \int w(\boldsymbol{v}) \exp\left[-{\rm i}\theta^{(\rm II)}\right] \\
&\quad \times H_1(t_1) H_2(t_2) H_3(t_3) H_2(t_4) H_1(t_5) \\
&\quad \times < u_2^*(t-t_5-\tau) u_3(t-t_4-t_5) \\
&\quad \times u_3^*(t-\tau-t_3-t_4-t_5) \\
&\quad \times u_2(t-t_2-t_3-t_4-t_5) > {\rm d}\Sigma_2, \quad (4)
\end{aligned}
$$

where, $A = S_1(\boldsymbol{r})\exp[-{\rm i}(\omega_1 t + \omega_2\tau)]$; $B = S_2(\boldsymbol{r})\exp\{-{\rm i}[\omega_1 t + (\omega_2+\omega_3)\tau]\}$; $S_1(\boldsymbol{r}) = -\dfrac{{\rm i}N\mu_1^2\mu_2^2}{\hbar^3}\varepsilon_1\varepsilon_2(\varepsilon_2')^* \exp\{{\rm i}[\boldsymbol{k}_1+\boldsymbol{k}_2-\boldsymbol{k}_2']\cdot\boldsymbol{r}\}$; $S_2(\boldsymbol{r}) = \dfrac{{\rm i}N\mu_1^2\mu_2^2\mu_3^2}{\hbar^5}\varepsilon_1\varepsilon_2\varepsilon_3(\varepsilon_3')^*(\varepsilon_2')^* \exp\{{\rm i}[\boldsymbol{k}_1+\boldsymbol{k}_2-\boldsymbol{k}_2'+\boldsymbol{k}_3-\boldsymbol{k}_3']\cdot\boldsymbol{r}\}$; $\theta^{(\rm I)} = \boldsymbol{v}[\boldsymbol{k}_1(t_1+t_2+t_3)+\boldsymbol{k}_2(t_2+t_3)-\boldsymbol{k}_2' t_3]$; $\theta^{(\rm II)} = \boldsymbol{v}[\boldsymbol{k}_1(t_1+t_2+t_3+t_4+t_5)+\boldsymbol{k}_2(t_2+t_3+t_4+t_5)-\boldsymbol{k}_3'(t_3+t_4+t_5)+\boldsymbol{k}_3(t_4+t_5)-\boldsymbol{k}_2' t_5]$; $H_1(t) = {\rm e}^{-d_1 t}$; $H_2(t) = {\rm e}^{-d_2 t}$; $H_3(t) = {\rm e}^{-d_3 t}$; $d_1 = \Gamma_{10} + {\rm i}\Delta_1$; $d_2 = \Gamma_{20} + {\rm i}\Delta_a$; $d_2^* = \Gamma_{20} - {\rm i}\Delta_a$; $d_3 = \Gamma_{30} + {\rm i}\Delta_b$; $\Delta_a = \Delta_1 + \Delta_2$; $\Delta_b = \Delta_1 + \Delta_2 + \Delta_3$; $\mu_1(\mu_2,\ \mu_3)$ and $\Gamma_{10}(\Gamma_{20},\ \Gamma_{30})$ are the dipole-moment matrix element and the transverse relaxation rate of the transition between $|0\rangle$ and $|1\rangle$ ($|1\rangle$ and $|2\rangle$, $|2\rangle$ and $|3\rangle$), respectively. The detunings are represented by $\Delta_1 = \Omega_1 - \omega_1$, $\Delta_2 = \Omega_2 - \omega_2$ and $\Delta_3 = \Omega_3 - \omega_3$. $\int {\rm d}\Sigma_1$ is defined as the four-fold integration: $\int {\rm d}\Sigma_1 = \int_{-\infty}^{+\infty} {\rm d}v \int_0^{+\infty} {\rm d}t_3 \int_0^{+\infty} {\rm d}t_2 \int_0^{+\infty} {\rm d}t_1$ and $\int {\rm d}\Sigma_2$ is defined as $\int {\rm d}\Sigma_2 = \int_{-\infty}^{+\infty} {\rm d}v \int_0^{+\infty} {\rm d}t_5 \int_0^{+\infty} {\rm d}t_4 \int_0^{+\infty} {\rm d}t_3 \int_0^{+\infty} {\rm d}t_2 \int_0^{+\infty} {\rm d}t_1$.

3. Nonlinear response at field level

In lifetime-broadened atoms (Doppler-free approximation $\boldsymbol{k}_i\cdot\boldsymbol{v} \approx 0$ and $\boldsymbol{k}_i'\cdot\boldsymbol{v} \approx 0$) the polarization expressions (3) and (4) of FWM and SWM reduce to

(i) when $\tau < 0$

$$P_{\rm F} = A\frac{1}{d_1^2}\frac{\exp[\alpha_2\tau]}{\alpha_2+d_2}, \quad (5)$$

$$P_{\rm S} == \frac{B\exp[(\alpha_2+\alpha_3)\tau]}{d_1^2[\alpha_2+d_2]^2[\alpha_2+\alpha_3+d_3]}, \quad (6)$$

(ii) when $\tau > 0$

$$P_{\rm F} = \frac{A}{d_1^2}\left(\frac{{\rm e}^{-\alpha_2\tau}-{\rm e}^{-d_2\tau}}{d_2-\alpha_2} + \frac{{\rm e}^{-d_2'\tau}}{d_2+\alpha_2}\right), \quad (7)$$

$$
\begin{aligned}
P_{\rm S} = B\Bigg\{ & \frac{-{\rm e}^{-(\alpha_2+\alpha_3)\tau}}{d_1^2(\alpha_2-d_2)^2(\alpha_2+\alpha_3-d_3)} + {\rm e}^{-(\alpha_3+d_2)\tau}\Bigg[\frac{(d_2-3\alpha_2)\tau}{d_1^2[\alpha_2^2-d_2^2](\alpha_3+d_2-d_3)} \\
& - \frac{2\alpha_2[\alpha_2^2-d_2(2\alpha_3+3d_2-2d_3)]}{d_1^2(\alpha_2^2-d_2^2)^2(\alpha_3+d_2-d_3)^2}\Bigg] + {\rm e}^{-d_3\tau}\Bigg[\frac{1}{d_1^2(\alpha_2+d_2)^2}\Bigg(\frac{\alpha_2+\alpha_3+2d_2-d_3}{(\alpha_3+d_2-d_3)^2} \\
& + \frac{1}{\alpha_2+\alpha_3+d_3}\Bigg) + \frac{1}{d_1^2(\alpha_3+d_2-d_3)^2(\alpha_2+\alpha_3-d_3)}\Bigg]\Bigg\}. \quad (8)
\end{aligned}
$$

When $\tau < 0$ expressions (7) and (8) present that both $P_{\rm F}$ and $P_{\rm S}$ show light response only (with ${\rm e}^{\alpha_2\tau}$ and ${\rm e}^{(\alpha_2+\alpha_3)\tau}$ being τ-dependent decay factors). However expressions (5) and (6) indicate that when $\tau > 0$, both $P_{\rm F}$ and $P_{\rm S}$ with radiation-matter detuning oscillation (RDO) terms (Table 1(a)) show both atom and light responses together (with ${\rm e}^{-d_2\tau}$, ${\rm e}^{-d_2'\tau}$ and ${\rm e}^{-(\alpha_3+d_2)\tau}$, ${\rm e}^{-d_3\tau}$ being τ-dependent decay factors). Specially, with RDO terms the NDFWM and SWM spectra are not symmetrical with respect to $\tau = 0$. Figures 3(a) and 3(b) present the NDFWM and SWM signal intensities versus time delay $\Gamma_{10}\tau$. Here, the maximum of the signal intensity is normalized to 1. The figures show that when $\tau > 0$ there are dramatic RDOs with many terahertz detuning frequencies shown in Table 1(b).

Table 1(a). RDO frequency terms of the polarizations of NDFWM and SWM.

	NDFWM($P_{\rm F}$)		SWM($P_{\rm S}$)	
time delay	$\tau > 0$	$\tau < 0$	$\tau > 0$	$\tau < 0$
frequency terms	$-\omega_2$, $-\omega_2 \pm (\Delta_1+\Delta_2)$	$-\omega_2$	$-(\omega_2+\omega_3)$, $-(\omega_2+\omega_3)-(\Delta_1+\Delta_2)$, $-(\omega_2+\omega_3)-(\Delta_1+\Delta_2+\Delta_3)$	$-(\omega_2+\omega_3)$

Table 1(b). Asymmetry and RDO frequencies of the NDFWM and SWM signal intensities versus time delay τ.

	NDFWM($\lvert P_{\rm F}\rvert^2$)				SWM($\lvert P_{\rm S}\rvert^2$)			
	RDO	Asymmetry			RDO	Asymmetry		
time delay	$\tau > 0$	$\tau < 0$	$\tau > 0$	$\tau < 0$	$\tau > 0$	$\tau < 0$	$\tau > 0$	$\tau < 0$
frequency and asymmetry	$\left(\Delta_1^+ \Delta_2\right)$, $2\left(\Delta_1^+ \Delta_2\right)$	No	Yes	No	$(\Delta_1 + \Delta_2)$, $(\Delta_1 + \Delta_2 + \Delta_3)$, Δ_3	No	Yes	No

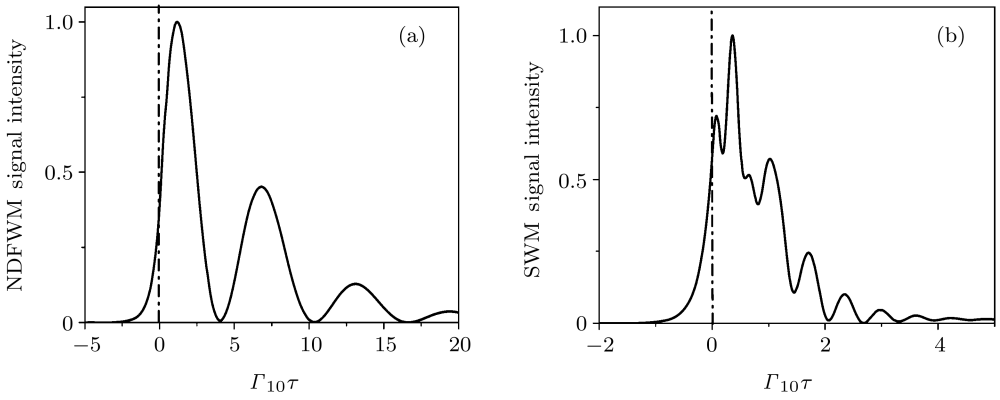


Fig.3. NDFWM $|P_{\rm F}|^2$ with asymmetry with respect to $\tau = 0$ and RDO for $\Delta_1/\Gamma_{10} = 0.15$, $\Delta_2/\Gamma_{10} = 0.4$, $\alpha_2/\Gamma_{10} = 0.1$ and $\alpha_3/\Gamma_{10} = 0.1$ (a) and SWM $|P_{\rm S}|^2$ with asymmetry with respect to $\tau = 0$ and RDO for $\Delta_1/\Gamma_{10} = 6$, $\Delta_2/\Gamma_{10} = 5$, $\Delta_3/\Gamma_{10} = 10$, $\alpha_2/\Gamma_{10} = 1$, and $\alpha_3/\Gamma_{10} = 1.5$ (b), with the Doppler effect neglected, $\Gamma_{20}/\Gamma_{10} = 0.1$, $\Gamma_{30}/\Gamma_{10} = 0.1$, and the maximum of the signal intensity normalized to 1.

The NDFWM and SWM complex susceptibilities $\chi_{\rm F}$ and $\chi_{\rm S}$ are obtained from the polarizations $P_{\rm F}$ and $P_{\rm S}$, respectively, as follows:

(i) when $\tau < 0$

$$\chi_{\rm F} = \frac{P_{\rm A}}{\varepsilon_0 < E_2(E_2')^* > E_1} = \frac{\psi_{\rm F}}{d_1^2(d_2 + \alpha_2)}, \quad (9)$$

$$\chi_{\rm S} = \frac{P_{\rm B}}{\varepsilon_0 < E_2(E_2')^* E_3(E_3')^* > E_1} = \frac{\psi_{\rm S}}{d_1^2[\alpha_2 + d_2]^2[\alpha_2 + \alpha_3 + d_3]}, \quad (10)$$

(ii) when $\tau > 0$

$$\chi_{\rm F} = \frac{P_{\rm A}}{\varepsilon_0 < E_2(E_2')^* > E_1} = \frac{\psi_{\rm F}}{d_1^2}\left\{\frac{1 - \exp\{-(d_2 - \alpha_2)\tau\}}{d_2 - \alpha_2} + \frac{\exp\{-(d_2' - \alpha_2)\tau\}}{d_2 + \alpha_2}\right\}, \quad (11)$$

$$\chi_{\rm S} = \frac{P_{\rm B}}{\varepsilon_0 < E_2(E_2')^* E_3(E_3')^* > E_1}$$
$$= \psi_{\rm S} {\rm e}^{(\alpha_2+\alpha_3)\tau}\left\{\frac{-{\rm e}^{-(\alpha_2+\alpha_3)\tau}}{d_1^2(\alpha_2 - d_2)^2(\alpha_2 + \alpha_3 - d_3)} + {\rm e}^{-(\alpha_3+d_2)\tau}\left[\frac{-2\alpha_2^2 + d_2(\alpha_3 + d_2 - d_3) + \alpha_2(\alpha_3 + 3d_2 - d_3)}{d_1^2(\alpha_2 - d_2)^2(\alpha_2 + d_2)(\alpha_3 + d_2 - d_3)^2}\right.\right.$$
$$\left. - \frac{d_2 - \alpha_2[1 + 2\tau(\alpha_2 + d_2)]}{d_1^2(-\alpha_2 + d_2)(\alpha_2 + d_2)^2(\alpha_3 + d_2 - d_3)}\right] + {\rm e}^{-d_3\tau}\left[\frac{1}{d_1^2(\alpha_2 + d_2)^2}\left(\frac{\alpha_2 + \alpha_3 + 2d_2 - d_3}{(\alpha_3 + d_2 - d_3)^2} + \frac{1}{\alpha_2 + \alpha_3 + d_3}\right)\right.$$
$$\left.\left. + \frac{1}{d_1^2(\alpha_3 + d_2 - d_3)^2(\alpha_2 + \alpha_3 - d_3)}\right]\right\}, \quad (12)$$

where $\psi_{\rm F} = -{\rm i}\,N\,\mu_1^2\,\mu_2^2/\,\varepsilon_0\,\hbar^3$ and $\psi_{\rm S} = {\rm i}\,N\,\mu_1^2\,\mu_2^2\,\mu_3^2/\varepsilon_0\hbar^5$.

The complex susceptibilities are greatly modified by the colour-locked noisy fields. Specifically, $\chi_{\rm F}$ and $\chi_{\rm S}$ strongly depend on the line width α_i and τ in broadband, while they become independent of them in narrowband. In the cw limit ($\alpha_i = 0$), the imaginary part and the real part of $\chi_{\rm F}$ and $\chi_{\rm S}$ can correspond to non-modified nonlinear absorption and dispersion. For the absorption curves, positive (negative) values indicate absorption (gain). Close inspection of Eq.(10) shows that for $\tau < 0$ when α_3/Γ_{10} controllably reduces to the cw case ($\alpha_3 = 0$), the absorption will increase (Fig.4(a)), and the slope of the normal dispersion curve will dramatically increase near resonance $\Delta_3/\Gamma_{10} = 0$, too (Fig.4(b)). The absorption and dispersion for $\tau > 0$ have the reverse behaviours with respect to those for $\tau < 0$. The absorption and the slope of the dispersion curve will decrease with α_3/Γ_{10} decreasing (Figs.4(c) and 4(d)). Moreover, the NDFWM and the SWM complex susceptibilities $\chi_{\rm F}$ and $\chi_{\rm S}$ show atom and light responses together. Figures 4(c) and 4(d) present RDO versus Δ_3/Γ_{10} and the RDO is dramatically improved with decreasing α_3/Γ_{10}. The RDO frequencies of the NDFWM and the SWM dispersion and absorption versus Δ_3/Γ_{10} are listed in Table 1(c).

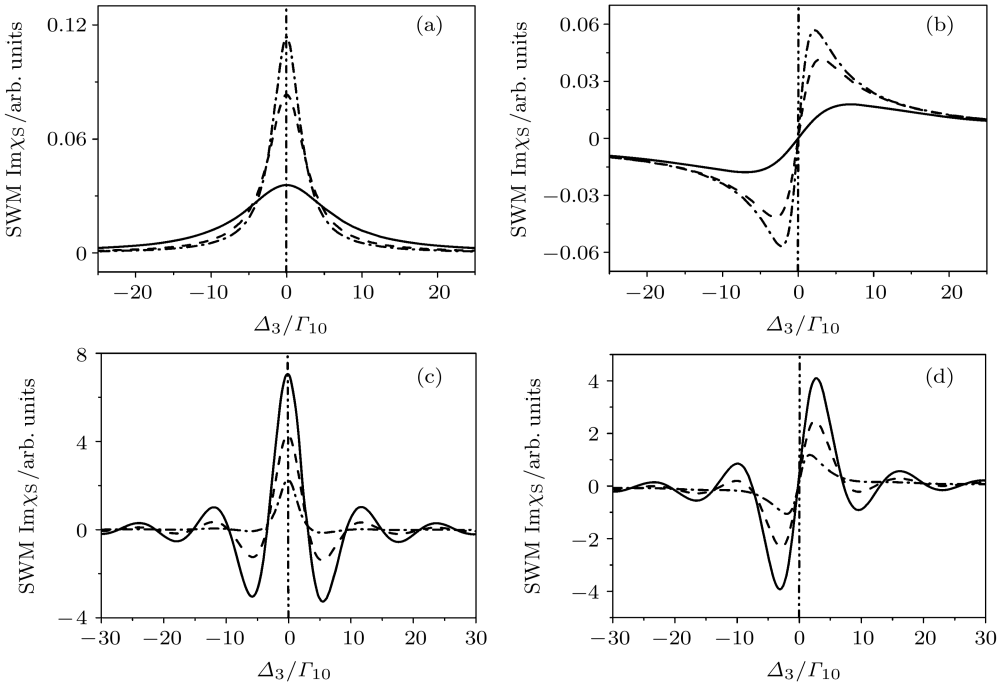


Fig.4. Nonlinear absorption ((a) and (c)) and dispersion ((b) and (d)) versus Δ_3/Γ_{10} for Eqs.(10) and (12) with $\Gamma_{20}/\Gamma_{10} = 0.1$, $\Gamma_{30}/\Gamma_{10} = 0.1$, $\Delta_1/\Gamma_{10} = \Delta_2/\Gamma_{10} = 0$, and $\alpha_2/\Gamma_{10} = 1$ for the values of α_3/Γ_{10} : 5 (solid curve), 1 (dash curve), 0.2 (dot-dash curve) in (a) and (b); for $\Gamma_{10}\tau = 0.525$, and the values of $\alpha_3/\Gamma_{10} = 5:5$ (solid curve), 3.5 (dash curve), 1 (dot-dash curve) in (c); for $\Gamma_{10}\tau = 0.472$ and the values of α_3/Γ_{10} : 5 (solid curve), 3.5 (dash curve), and 1 (dot-dash curve) in (d).

Table 1(c). RDO frequencies of complex susceptibility of NDFWM and SWM versus Δ_3/Γ_{10}.

	NDFWM($\chi_{\rm F}$)		SWM($\chi_{\rm S}$)	
time delay	$\tau > 0$	$\tau < 0$	$\tau > 0$	$\tau < 0$
Doppler free	0	0	$\Gamma_{10}\tau$	0

The expression for $\chi_{\rm B}$ is responsible for the modification to the non-modified nonlinear absorption-dispersion profile. The phase dispersion $\theta_{\rm F} = \tan^{-1}({\rm Im}\chi_{\rm F}/{\rm Re}\chi_{\rm F})$ of $\chi_{\rm F} = |\chi_{\rm F}|\,{\rm e}^{{\rm i}\theta_{\rm F}}$ and $\theta_{\rm S} = \tan^{-1}({\rm Im}\chi_{\rm S}/{\rm Re}\chi_{\rm S})$ of $\chi_{\rm S} = |\chi_{\rm S}|\,{\rm e}^{{\rm i}\theta_{\rm S}}$ can be obtained simply from Eqs.(9)–(12).

4. Nonlinear response at intensity level

The phase-sensitive detection of three-photon SWM is based on the polarization interference between NDFWM and SWM processes. Since optical fields oscillate too quickly for direct detection, they must be measured by beating with another field with

the same frequency. There are two ways to measure the nonlinear susceptibility of SWM experimentally. The first way is the conventional detection in which the SWM polarization $P_{\rm S}$ is measured at its own absolute square, $P_{\rm S}(P_{\rm S})^*$. The three-photon SWM signal intensity is proportional to $|\chi_{\rm S}|^2$ and all phase information of $\chi_{\rm S}$ has been lost. The second way to measure $\chi_{\rm S}$ is to introduce another NDFWM polarization $P_{\rm F}$ (called a reference signal or local oscillator) designed in frequency and wave vector to conjugate in its complex representation with the $P_{\rm S}$ polarization of interest. Thus, in this heterodyne case, the signal photons are derived from $(P_{\rm F}+P_{\rm S})[(P_{\rm F})^*+(P_{\rm S})^*]$ or $I_{\rm heterodyne}\propto\chi_{\rm S}$ (the signal is linear rather than quadratic). In heterodyne detected FWM, phase information is retained and one can take a full measurement of the complex susceptibility, including its phase. The FSPB intensity can be obtained as follows:

$$\begin{aligned} I(\tau,\Delta_i,\alpha_i) &\propto P_{\rm F}P_{\rm F}^*+P_{\rm F}P_{\rm S}^*+P_{\rm S}P_{\rm F}^*+P_{\rm S}P_{\rm S}^* \\ &= \eta_1|\chi_{\rm F}|^2\,{\rm e}^{-2\alpha_2|\tau|}+\eta_2|\chi_{\rm S}|^2\,{\rm e}^{-2(\alpha_2+\alpha_3)|\tau|} \\ &\quad +2\eta_{12}|\chi_{\rm F}||\chi_{\rm S}|\,{\rm e}^{-(2\alpha_2+\alpha_3)|\tau|} \\ &\quad \times\cos(\theta_{\rm F}-\theta_{\rm S}+\theta_R), \end{aligned} \tag{13}$$

where $\chi_{\rm F}=|\chi_{\rm F}|\,{\rm e}^{{\rm i}\theta_{\rm F}}=|\chi_{\rm F}|\cos\theta_{\rm F}+{\rm i}\,|\chi_{\rm F}|\sin\theta_{\rm F}$, $\chi_{\rm S}=|\chi_{\rm S}|\,{\rm e}^{{\rm i}\theta_{\rm S}}=|\chi_{\rm S}|\cos\theta_{\rm S}+{\rm i}\,|\chi_{\rm S}|\sin\theta_{\rm S}$, $\theta_{\rm R}=\Delta\boldsymbol{k}\cdot\boldsymbol{r}+\omega_3\tau$, $\Delta\boldsymbol{k}=\boldsymbol{k}_3'-\boldsymbol{k}_3$, $\eta_1=\varepsilon_0^2\varepsilon_1^2\varepsilon_2^2(\varepsilon_2')^2$, $\eta_2=\varepsilon_0^2\varepsilon_1^2\varepsilon_2^2(\varepsilon_2')^2\varepsilon_3^2(\varepsilon_3')^2$ and $\eta_{12}=\varepsilon_0^2\varepsilon_1^2\varepsilon_2^2(\varepsilon_2')^2\varepsilon_3^(\varepsilon_3')^*$. Equation (13) shows that three types of signals contribute to the FSPB intensity. They are the NDFWM signal induced by $\chi_{\rm F}$, the SWM signal induced by $\chi_{\rm S}$ and the coherent signal induced by $\chi_{\rm F}$ and $\chi_{\rm S}$. The NDFWM and SWM signals present terahertz detuning frequencies without ω_3 term listed in Table 2. The coherent signal presents the oscillation on a femtosecond time scale with ω_3 term listed in Table 2. It means that the FSPB is induced by the coherence between NDFWM and SWM. Figure 5(a) presents the FSPB signal intensity versus $\Gamma_{10}\tau$ for $\alpha_2/\Gamma_{10}=10$, $\alpha_3/\Gamma_{10}=4$, $\Delta_{20}/\Gamma_{10}=0.1$, $\Delta_{30}/\Gamma_{10}=0.1$, $\omega_3/\Gamma_{10}=30$, and $\Delta_{10}/\Gamma_{10}=0.5$ (solid curve). In this figure there exist two types of oscillations with different frequencies apparently. Moreover, Fig.5(b) is the fast Fourier transform (FFT) of FSPB spectrum curve. It shows two groups of frequencies. The low frequency group corresponds to RDO terahertz detuning frequencies, and the high frequency group corresponds to polarization beat on a femtosecond time scale. All the oscillation frequencies are listed in Table 2. From the list we can see high frequency with component ω_3 and low frequency with component detuning terms $\Sigma\Delta_i$. Meanwhile, when $\tau<0$ there exists only the polarization beat with one high frequency ω_3, while when $\tau>0$ there exist the polarization beat and RDO with many high and low frequencies. Thus when $\tau<0$ the FSPB signal only shows the light response to the polarization beat form, while when $\tau>0$ the signal shows the interplay between the material and light responses to both polarization beat and RDO forms.

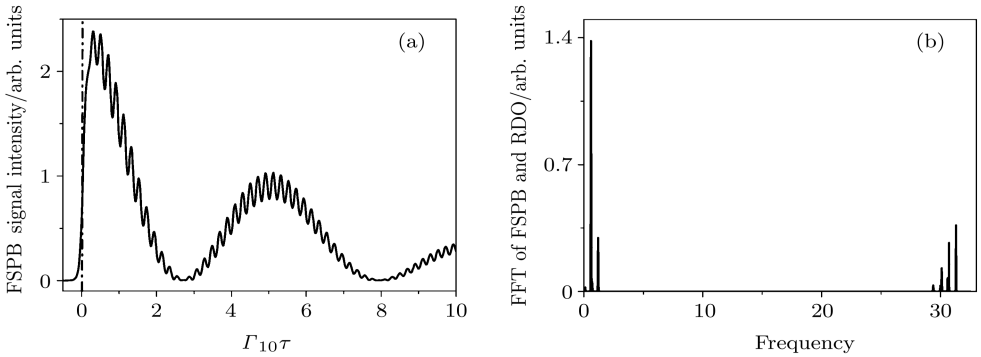


Fig.5. FSPB, RDO, and their Fourier transforms, where the FSPB signal intensity versus $\Gamma_{10}\tau$ with $\alpha_2/\Gamma_{10}=10$, $\alpha_3/\Gamma_{10}=4$, $\Delta_{20}/\Gamma_{10}=0.1$, $\Delta_{30}/\Gamma_{10}=0.1$, $\omega_3/\Gamma_{10}=30$, and $\Delta_{10}/\Gamma_{10}=0.5$ is shown in (a) and the FFT of FSPB and RDO for solid curve is indicated in (b).

Table 2. Polarization beat frequencies and RDO frequencies of the FSPB signal intensity.

FSPB between NDFWM and SWM			
time delay	$\tau>0$	$\tau<0$	combination of $\tau>0$ and $\tau<0$
frequency	$(\Delta_1^+\Delta_2)$, $2(\Delta_1^+\Delta_2)$, $(\Delta_1+\Delta_2+\Delta_3),\Delta_3$, $\omega_3+(\Delta_1+\Delta_2)$, $\Omega_3+\Delta_1+\Delta_2,\omega_3$, $\omega_3+2(\Delta_1+\Delta_2)$, $\Omega_3,\Omega_3+2\Delta_1+2\Delta_2,\omega_3-(\Delta_1+\Delta_2)$	ω_3	$(\Delta_1^+\Delta_2)$, $2(\Delta_1^+\Delta_2)$, $(\Delta_1+\Delta_2+\Delta_3)$, Δ_3, $\omega_3+(\Delta_1+\Delta_2)$, $\Omega_3+\Delta_1+\Delta_2$, ω_3, Ω_3, $\omega_3+2(\Delta_1+\Delta_2)$, $\Omega_3+2\Delta_1+2\Delta_2$, $\omega_3-(\Delta_1+\Delta_2)$

Although the complex susceptibilities (nonlinear responses) are greatly modified by the colour-locked noisy fields, they can still be obtained effectively in an ideal limit. The higher-order nonlinear optical processes are usually much smaller in amplitude than the lower order ones. In the heterodyne detection, we may assume that $|P_{\rm F}|^2 \gg |P_{\rm S}|^2$ at intensity level ($|\chi_{\rm F}| \gg |\chi_{\rm S}|$ at field level), so the reference signal (NDFWM) originating from the ω_2 frequency components of the twin beams 2 and 3 is much larger than the SWM signal arising from the ω_2 and ω_3 frequency components of the twin beams 2 and 3 as shown below:

$$\begin{aligned} & I(\tau, \Delta_i, \alpha_i) \\ \propto\ & P_{\rm F}P_{\rm F}^* + P_{\rm F}P_{\rm S}^* + P_{\rm S}P_{\rm F}^* \\ =\ & \eta_1 |\chi_{\rm F}|^2 {\rm e}^{-2\alpha_2|\tau|} + 2\eta_{12} |\chi_{\rm F}| |\chi_{\rm S}| \\ & \times {\rm e}^{-(2\alpha_2+\alpha_3)|\tau|} \cos(\theta_{\rm F} - \theta_{\rm S} + \theta_{\rm R}). \end{aligned} \tag{14}$$

Equation (14) indicates that the FSPB signal of heterodyne detection is modulated with frequency ω_3 as τ varies. Owing to the high frequency factor ω_3 of $\theta_{\rm R}$ the phase coherent control of light beams in FSPB is subtle. The phase of the FSPB signal strongly depends on the phase angle $\theta_{\rm S}$ of $\chi_{\rm S}$. Such a FSPB can effectively be employed via optical heterodyne detection to yield the real and the imaginary parts of $\chi_{\rm S}$. If we adjust the time delay τ and $\boldsymbol{r}$ such that $\theta_{\rm F} + \theta_{\rm R} = 2n\pi$ (i.e. $\tau = [2n\pi - \theta_{\rm F}(\tau) - \Delta\boldsymbol{k}\cdot\boldsymbol{r}]/\omega_3$, $\Delta\boldsymbol{k}\cdot\boldsymbol{r} = 0$, and the value of integer n depends on the sign of τ sensitively), then

$$\begin{aligned} I(\Delta_3) \propto\ & \eta_1 |\chi_{\rm F}|^2 {\rm e}^{-2\alpha_2|\tau|} + 2\eta_{12} {\rm e}^{-(2\alpha_2+\alpha_3)|\tau|} \\ & \times |\chi_{\rm F}| \,{\rm Re}[\chi_{\rm S}(\Delta_3)]. \end{aligned} \tag{15}$$

However, if $\theta_{\rm F} + \theta_{\rm R} = (2n + 1/2)\pi$ (i.e. $\tau = [2n\pi + \pi/2 - \theta_{\rm F}(\tau) - \Delta\boldsymbol{k}\cdot\boldsymbol{r}]/\omega_3$, and $\Delta\boldsymbol{k}\cdot\boldsymbol{r} = 0$), we have

$$\begin{aligned} I(\Delta_3) \propto\ & \eta_1 |\chi_{\rm F}|^2 {\rm e}^{-2\alpha_2|\tau|} + 2\eta_{12} {\rm e}^{-(2\alpha_2+\alpha_3)|\tau|} \\ & \times |\chi_{\rm F}| \,{\rm Im}[\chi_{\rm S}(\Delta_3)]. \end{aligned} \tag{16}$$

In other words, by changing the time delay τ between components in beams 2 and 3, we can obtain the real and the imaginary parts of $\chi_{\rm S}(\Delta_3)$ (Figs.6(a) and 6(b)). The subtle value of τ is generally determined by the gradual approach method from $\theta_{\rm F}(\tau)+\theta_{\rm R}(\tau) = 2n\pi$ or $(2n+1/2)\pi$. Owing to adding the local oscillator intensity to Eqs.(15) and (16), Figs.6(a) and 6(b) show the positive values of absorption and dispersion profiles compared with the solid curves in Figs.4(c)

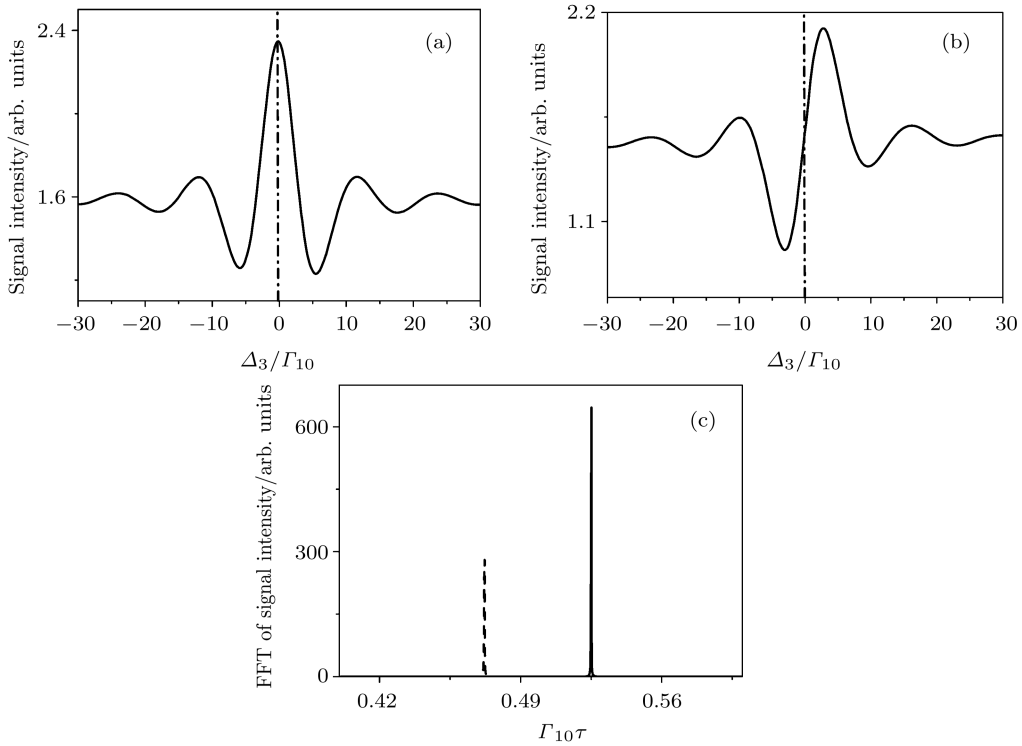


Fig.6. The heterodyne detection spectra versus Δ_3/Γ_{10} of the FSPB with $\Gamma_{20}/\Gamma_{10} = 0.1$, $\Gamma_{30}/\Gamma_{10} = 0.1$, $\Delta_1/\Gamma_{10} = 0.01$, $\Delta_2/\Gamma_{10} = 0.02$, $\alpha_2/\Gamma_{10} = 1$, $\alpha_3/\Gamma_{10} = 5$ and $\omega_3/\Gamma_{10} = 30$, in which the nonlinear dispersion profile is presented when $\Gamma_{10}\tau = 0.525$ in (a), the absorption profile when $\Gamma_{10}\tau = 0.472$ is shown in (b) and the FFT of heterodyne detected signal curve is indicated in (c) for the values of $\Gamma_{10}\tau$: 0.525 (solid curve) and 0.472 (dash curve).

and 4(d). Figure 6(c) shows the FFT of the heterodyne detection spectra in Figs.6(a) and 6(b). It means that those spectra each have one oscillation frequency and these frequencies are different from each other.

5. Discussion and conclusion

Ma *et al* [14] have reported the application of the FSPB induced by the third-order susceptibility $\chi^{(3)}$ to measuring the phase of $\chi^{(3)}$ in a filmy solid, they obtain the phase through simultaneously recording the signal beams radiating in the two different directions to obtain the difference in phase.

We have studied the colour-locked twin-noisy-field correlation effects in the fifth-order nonlinear susceptibility of ultrafast polarization beats in a cascade four-level system. More importantly, the effects are exploited as the fifth-order phase-sensitive heterodyne detection of ultrafast polarization beats. The fifth-order nonlinear response can be controlled and modified through the colour-locked correlation with twin noisy fields. Thus, such a method is a good way to measure the real and the imaginary parts and the phase dispersion of the fifth-order nonlinear susceptibility.

References

[1] Harris S E 1997 *Phys. Today* **50**(7) 36

[2] Lu B, Burkett W H and Xiao M 1998 *Opt. Lett.* **23** 804
Zhang Y P, Brown A W and Xiao M 2007 *Opt. Lett.* **32** 1120
Zhang Y P and Xiao M 2007 *Appl. Phys. Lett.* **90** 111104

[3] Zhang Y P, Gan C L and Xiao M 2006 *Phys. Rev.* A **73** 053801

[4] Wu H B, Chang H, Ma J, Xie C D and Wang H 2005 *Acta Phys. Sin.* **54** 8 (in Chinese)

[5] Gao J Y, Su X M, Wang L J and Zhuo Z C 2002 *Chin. Phys.* **11** 35

[6] Gan C L, Zhang Y P, Yu X J, Nie Z Q, Li L, Song J P, Ge H, Jiang T, Zhang X C and Lu K Q 2007 *Acta Phys. Sin.* **56** 5 (in Chinese)

[7] Zuo Z C, Sun J, Liu X, Mi X, Yu Z H, Jiang Q, Fu P M, and Wu L A 2007 *Chin. Phys.* **16** 1042

[8] Wang H, Goorskey D and Xiao M 2001 *Phys. Rev. Lett.* **87** 073601

[9] Wu Y 2005 *Phys. Rev.* A **71** 053820
Wu Y and Deng L 2004 *Opt. Lett.* **29** 1144

[10] Zhang Y P, Gan C L, Li L, Ma R Q, Song J P, Jiang T, Yu X J, Li C S, Ge H and Lu K Q 2005 *Phys. Rev.* A **72** 013812

[11] Zhang Y P, de Araujo C B and Eyler E E 2001 *Phys. Rev.* A **63** 043802

[12] Fu P M, Mi X, Yu Z H, Jiang Q, Zhang Y P and Li X F 1995 *Phys. Rev.* A **52** 4867

[13] Ulness D 2003 *J. Phys. Chem.* A **107** 8111
Schulz T F, Aung P P, Weisel L R, Cosert K M, Gealy M W and Ulness D J 2005 *J. Opt. Soc. Am.* B **22** 1052

[14] Ma H, Acioli L H, Gomes A S and de Araujo C B 1991 *Opt. Lett.* **16** 603
Ma H and de Araujo C B 1993 *Phys. Rev. Lett.* **71** 3649